Available online at www.sciencedirect.com

SciVerse ScienceDirect

Procedia Environmental Sciences 19 (2013) 436 – 445

Procedia Environmental Sciences

Four Decades of Progress in Monitoring and Modeling of Processes in the Soil-Plant-Atmosphere System: Applications and Challenges

A geostatistical approach to estimate soil moisture as a function of geophysical data and soil attributes

Daniela De Benedetto[a,b*], Annamaria Castrignanò[b], Ruggiero Quarto[a]

[a] *Dipartimento di Scienze della Terra e Geoambientali, University of Bari, Aldo Moro, Italy*
[b] *Consiglio per la Ricerca e la Sperimentazione in Agricoltura, Research Unit for Cropping Systems in Dry Environments, Bari, Italy*

Abstract

Successful implementation of site-specific irrigation requires an understanding of within-field-variability of soil parameters. These parameters can be estimated by direct sampling or by indirect surveying using geophysical data. The geophysical outputs are quite sensitive to soil water content; therefore, they can be used as covariates in soil water content (SWC) estimation.
The objectives of this study were to use geophysical and soil data as auxiliary variables in the estimation of soil water content through geostatistical techniques.
The surveys were carried out in a test site at the agricultural experimental farm located in south-eastern Italy in dry and wet soil conditions. The plot was surveyed with an EMI sensor and two different mono-static GPR systems, one with central frequencies of 600/1600 MHz and the other with a central frequency of 250MHz. Forty-eight soil cores were collected for laboratory analysis of textural properties. One hundred and sixteen soil samples up to 0.30m-depth were collected to measure the SWC with gravimetric method. Kriging with external drift (KED), a non-stationary geostatistical technique, was used to estimate SWC with EMI, GPR and soil data as covariates. Cross-validation test was used to assess the goodness of the estimates and compare KED with ordinary kriging.
The results showed that the approach using the auxiliary variables can be preferred to univariate kriging in terms of correlation between true and estimated values and capability of interpretation of spatial variability. Kriging with external drift proved to be a valid tool in sensor data fusion and could be effectively applied in Precision Irrigation.

Keywords: GPR; EMI; Geostatistics; KED; water content

* Corresponding author. Tel.: +39-080-5475024.
E-mail address: daniela.debenedetto@virgilio.it

doi:10.1016/j.proenv.2013.06.050

1. Introduction

Assessment of soil water content (SWC) variation is quite critical in agricultural applications and actually agronomists and farmers need information about SWC variation in both spatial and temporal scales to manage irrigation practices efficiently. Measurement of SWC variability is complicated due to soil heterogeneity and various environmental variabilities. No single efficient method has been developed to map high or low soil moisture zones at the field scale without disturbing the soil [1]. Rapid assessment and monitoring of SWC over large areas are therefore necessary in order to achieve efficient water management at field scale. Gravimetric method is considered as the standard to measure SWC variation, but it is inefficient in providing large scale rapid data collection and is restricted to a small measurement volume. Geophysical methods, such as electromagnetic induction (EMI) and Ground Penetrating Radar (GPR), measure a larger sample volume and are capable to cover large areas efficiently, which cannot be obtained from other methods.

EMI methods measure apparent electrical conductivity (EC_a) in the soil that is recognised as a valuable geophysical measurement in agriculture for characterising spatial variability in soil at field and landscape scales [2]. EC_a can be intensively recorded, in an easy and inexpensive way, and is usually related to various soil physico-chemical properties across a wide range of soils. GPR is a high-resolution geophysical technique that utilizes the transmission and reflection of high frequency electromagnetic waves. Propagation velocity of radar wave depends mainly on soil permittivity, which is known to be strongly related to volumetric water content. GPR methods have been shown to be a viable alternative technique to monitor and evaluate shallow soil water content [3]. To estimate soil properties from GPR data, it needs firstly to look for which sensor output (amplitude, phase, envelope, etc.) is more closely correlated with them and then relate soil properties to that output statistically [4].

EC_a and amplitude of radar signal can be used to improve estimation of spatially variable water content, when they are spatially correlated. However, modeling the relationships between soil water content and geophysical output is not an easy task. This is due to the dependency of geophysical data on many soil properties, over different spatial scales, and in a very complex way. A way to combine different variables is assuming a spatial trend in the target variable, which is linearly related to the auxiliary variables [5-6]. The method, known as kriging with external drift (KED) in the scope of intrinsic random function of order k (IRF-k), introduces the concepts of generalised increments and generalised covariance and assumes that generalised increments produce a second-order stationary process [7-8].

The objectives of this study were to use geophysical and soil data as auxiliary variables in the estimation of soil water content through geostatistical techniques and to explore the capability of geostatistical methods to incorporate these auxiliary variables in the prediction under two different soil water conditions. Finally, cross-validation test was used to assess the prediction performance of kriging with external drift compared with ordinary kriging.

2. Material and methods

2.1. Study area and data collection

This experiment was conducted on a bare plot (40 m×20 m) in the experimental farm of CRA-SCA, located at Rutigliano-Bari (40° 59′ 48.25″ N, 17° 02′ 02.06″ E), in south-eastern Italy. Soil is classified as fine, mixed, superactive, thermic Typic Haploxeralfs according to the Soil Taxonomy [9]. Soil texture is mainly clayey with the clay content ranging from 30% to 60% by weight and basically increasing in depth. The bedrock is constituted of a layered sequence of Cretaceous limestone with some dolomitic limestone level and occurs at variable depth due to its irregularly shaped boundary.

Two sets of measurements were collected under two different soil water conditions, to capture the major variations in soil water content at the site. In July 2012, the surveys were performed in dry soil, since rainfall events did not occur in June and July and the average temperature exceeded 30°C. In October 2012, the plot was irrigated (drip irrigation) for a week until the saturation, and the surveys were carried out after water leaching for gravitation.

In both dates, the plot was surveyed with an EMI sensor (EM38DD, Geonics Limited, Mississauga, Ontario, Canada), which consists of two single coils positioned perpendicularly to each other, one orientated horizontally and the other one vertically. The sensor, carried across the plot, simultaneously measures apparent electrical conductivity (EC_a) in the two orientations, each having a different depth response profile [10]. EC_a measurements were geo-referenced using a Differential Global Positioning System (HiPer® 27 Pro, TOPCON) with planimetric and altimetric centimeter accuracies. The surveys were conducted along longitudinal and transversal transects about 1 m apart and data were recorded every second with a spatial resolution of 0.5 m on average along the transect. GPR data were collected on the EMI transects with the common offset reflection method, using two different monostatic GPR systems: one with a central frequency of 250MHz (Noggin 250 MHz, Sensors & Software Inc, Mississauga, Ontario, Canada), the other with two central frequencies of 600 and 1600MHz (IDS Ing-manufactured, RIS 2k-MF Multifrequency Array Radar-System). The 250MHz GPR system acquired the data using a time window of 100 ns with a sampling interval of 0.2ns and spacing between the traces of 0.05m. The 600 and 1600MHz GPR system worked with a time window of 60ns and a sampling interval of 0.05ns; successive traces were collected every 0.024m.

In order to evaluate some velocity profiles of the subsoil, we carried out measurements by means of the technique of Common Mid Point (CMP), through a bistatic GPR system with central frequency of 450 MHz (pulseEKKO 1000, Sensors & Software Inc, Mississauga, Ontario, Canada).

In all cases sixteen pulses for each measurement point were sent in the soil, for obtaining stacked traces less affected by noises.

Forty-eight geo-referenced soil samples were collected up to 0.30-m depth and analysed in laboratory for soil texture (sand, silt and clay expressed as weight percentage). One hundred and sixteen geo-referenced samples were collected up to 0.30-m depth at the nodes of a geophysical grid with spacing of 4 meters and the water content was calculated with gravimetric method at each date.

2.2. Data analysis

2.2.1. GPR data analysis

The GPR data pre-processing were performed with REFLEX Software [11] and included the set zero time correction, “dewow” filter and trapezoidal bandpass filter. No amplitude gain functions were applied to the data. After processing, the instantaneous amplitude or envelope of data was calculated using a quadrature filter (Hilbert transformation), which gives an estimation of the attenuation of radar signal, that might be caused by moisture conditions. Amplitude maps (time slices) were built averaging the amplitude of the radar signal within consecutive time windows of Δt width near the period related to the frequency of the antennas (4ns, 2ns and 1ns for 250MHz, 600 and 1600MHz antennas, respectively). The time slices were then transformed in depth slice maps using the velocity of the radar waves determined through the analysis of Common-Mid Point measurements with a bistatic system at the frequency of 450MHz (not reported). To eliminate the noise due to variable energy of the transmitted signal at different points, a normalization of the amplitudes was performed using as reference the first time slice, mainly related to the radar waves in air.

2.2.2. Geostatistical analysis

The geostatistical analysis can be split into parts: part A, aimed at estimation of all variables, and part B, aimed at showing the potential of geophysical and soil data as auxiliary variables in the estimation of soil water content.

Therefore, for the part A, the whole multi-sensor dataset was split into four groups for each date: 1) EC_a data; 2) GPR depth slices for each frequency; 3) soil textural properties and 4) soil water content. The variables, which showed significant departure from normal distribution, were previously transformed through gaussian anamorphosis. Geostatistical procedures were separately applied to each group of data by using a multivariate approach and fitting a linear model of coregionalization (LMC) to the experimental variograms. EC_a data and textural properties were interpolated with ordinary cokriging on a 0.5-m x 0.5-m grid. GPR data were interpolated with block cokriging through a regular 5x5 discretization of the block and using the previous grid. Soil water content was estimated using ordinary kriging. The geostatistical analyses were performed with ISATIS software [12].

2.2.3. Estimation of soil water content

For the part B, a subset of predictors of SWC at the each date was selected from the auxiliary variables using stepwise regression with a mixed (forwards and backwards) approach and the significance entry and stay levels for an auxiliary variable set at 0.15. The approach was performed with selection algorithm STEPWISE of software SAS [13]. The potential regression predictors were the EC_a in horizontal (EC_{aH}) and vertical (EC_{aV}) modes; the amplitude for 250 MHz frequency at four depths: from 0.12m to 0.30m with a step of 0.06m (Amp250MHz_0.12m-Amp250MHz_0.30m); the amplitude for 600MHz antenna at nine depths: from 0.06m to 0.30m with a step of 0.03m (Amp600MHz_0.06m-Amp600MHz_0.30m); the amplitude for 1600 MHz frequency at ten depths: from 0.03m to 0.165m with a step 0.015m (Amp1600MHz_0.03m-Amp1600MHz_0.165m); clay, fine and coarse silt, fine and coarse sand.

Kriging with external drift (KED) was used here in the scope of intrinsic random function of order k (IRF-k) theory, defined by Matheron because of the difficulties resulting from the simultaneous estimation and modelling of drift and variogram [14]. Estimation can be decomposed into two components: a slowly varying deterministic function, known as drift, and a rapidly fluctuating spatially correlated random component with zero mean. The basic hypothesis of KED is that expectation of a variable, known only at a small set of points, can be modelled as the sum of a basis of polynomials representing the internal drift and linear functions of secondary variables representing the external drift.

The correlation structure associated with the random part is expressed by a generalized covariance, GC(h), function of the separation distance (**h**) between two observations. The model used to express the generalized covariance was a polynomial model, namely a linear combination of a given set of generic basic structures under constraints on the coefficients:

$$GC(h)=C_0\,\delta(|\boldsymbol{h}|)-b_0|\boldsymbol{h}|+b_1|\boldsymbol{h}|^2 log|\boldsymbol{h}|+b_2|\boldsymbol{h}|^3 \quad (1)$$

where $\delta(|\mathbf{h}|)=0$ for $|\mathbf{h}|>0$ else $\delta(|\mathbf{h}|)=1$. In order that GC(h) be an authorized generalized covariance of an IRF-k, the coefficients C_0, b_0, b_1 must be positive and $b_2 \geq -3/2\sqrt{b_0 b_1}$ [15].

In IRF-k, structural analysis is performed in two stages: firstly the order, k, of drift is established and, secondly, the generalized covariance, GC(h), is estimated by fitting a parametric model. To determine the degree of drift, the least-squares errors are ranked in ascending magnitude at each target point, and the mean rank is computed for each order k over all estimated target points; the optimal degree of drift is that

with minimum mean rank. Once k is determined the operational criterion to select the optimal generalized covariance involves a ratio of mean square errors which should be close to 1 [15].

To apply this technique, it is necessary to know the predictors at all nodes of the interpolation grid. Therefore, the geostatistical estimates were used. The SWC content at the two dates was interpolated with KED at the nodes of the grid previously defined.

2.2.4. Comparison of kriging techniques

Comparison of the accuracy and precision of SWC estimates, obtained with ordinary kriging (OK) and KED was done using the cross-validation statistics as follows [16]. Let $Y_{[i]}$ be the observed response value removed at the i-th iteration; let $\hat{Y}_{[i]}$ be its corresponding prediction obtained by fitting the model to the remaining n-1 points; let $e[i]= Y_{[i]} - \hat{Y}_{[i]}$ be the difference between the observed and estimated values and let $\sigma_{[i]}$ be the mean squared prediction error of $\hat{Y}_{[i]}$; the three cross-validation statistics are:

$$CV_1 = \frac{1}{n}\sum_{i=1}^{n}\frac{e_{[i]}}{\sigma_{[i]}};CV_2 = \left(\frac{1}{n}\sum_{i=1}^{n}\frac{e_{[i]}^2}{\sigma_{[i]}^2}\right)^{\frac{1}{2}};CV_3 = \left(\frac{1}{n}\sum_{i=1}^{n}e_{[i]}^2\right)^{\frac{1}{2}} \quad (2)$$

CV_1 was used to assess the unbiasedness of prediction and the optimal value of CV_1 should be approximately zero; CV_2 was used to assess the accuracy of mean squared prediction error and should be approximately 1; CV_3 was used to check the goodness of prediction, and models with smaller values of CV_3 should be preferred, because this means that fitted values are close to observed values [16]. Moreover, to test the goodness of fit in the two approaches, the correlation coefficient (r) between observed and predicted values was calculated.

3. Results

The descriptive statistics of all data highlighted that the data distributions showed sensible departures from normal distribution, except SWC data, which justifies the data transformation by Gaussian anamorphosis. The variogram models for each group (not reported), generally reaveal the same basic structures at the two dates, with slight differences in the range, which means temporal persistency of the main structures of spatial dependence in the soil.

The cokriged maps of soil texture (Fig. 1) indicated that the main components were clay and silt, whereas sand content was generally very low. The plot could be roughly split into two main areas: the northern area characterized by lower clay content, whereas the middle and southern parts with generally higher clay content and lower coarse silt and sand content.

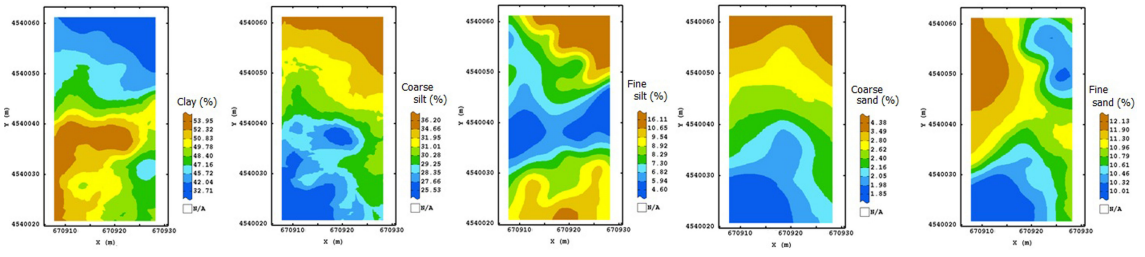

Fig. 1. Spatial estimate of soil texture (Color scale uses isofrequency classes).

3.1. Maps of July monitoring

The OK SCW map (Fig. 2a) showed approximately the same division observed in the soil maps with the northern area characterized by higher water content. The high degree of smoothness in this map is due to the coarser sampling scale.

The EC_a maps in the two polarization modes appeared quite similar (Fig. 3), which means that the soil profile was quite continuous up to approximately 1-m depth. In particular, a central area of the field with higher values of EC_a can be observed, corresponding approximately to the zones characterized by higher SWC and silt content.

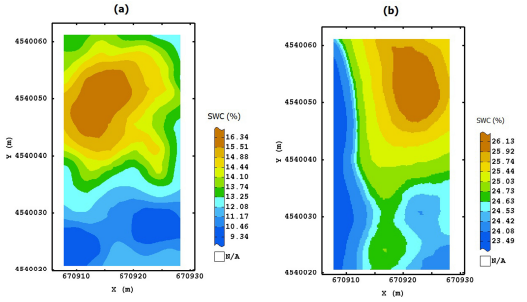

Fig. 2. Spatial estimate of SWC in July (a) and October monitoring (b) obtained with ordinary kriging.

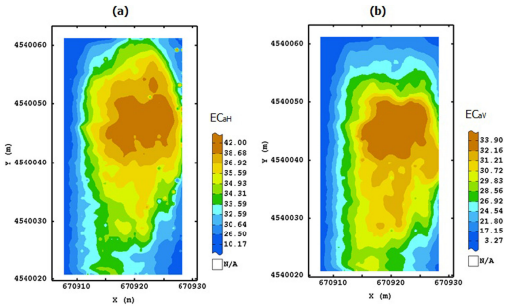

Fig. 3. Spatial estimate of EC_a in July monitoring in horizontal (a) and vertical (b) polarization (in milli-Simiens per meter).

Through analysis of CMP (not reported), two reflected signals were identified at approximately 10 and 24 ns, with corresponding velocities of 0.06 mns^{-1} and 0.11 mns^{-1}, respectively. These velocities were used to convert the time slices as depth slices. All GPR depth slices deeper than 0.30-m will not be treated from now onwards, in order to make the GPR maps comparable with the soil water content maps.

The maps of the estimated amplitude for 250MHz antenna at the investigated depths (Fig. 4) displayed some consistency along the whole profile, with tendentially higher values of amplitude along the north-eastern and south-western sides of the plot. The greater attenuation of GPR signal might be due to higher clay content (Fig. 2).

The maps of the estimated amplitude for 600 and 1600 MHz antenna (in Figs. 5-6 only the slices more representative are reported) were less smoothed (more noisy), compared with the ones of the 250 MHz antenna, because of their finer spatial resolution, and didn't show similar spatial structures. In particular the maps for 600MHz antenna, up to 0.18m depth (Fig. 5a, b), and the maps for 1600 MHz antenna (Fig. 6a) could be split into two blocks N-S oriented, with the western one characterized by higher values of amplitude. At deeper depth (Fig. 5c, d and Fig 6b, c), it was not possible to recognize well-defined spatial

structures. These differences might be due to short-range variability in micro-structures, which the GPR system at 250MHz antenna didn't seize because of its coarser spatial resolution. Moreover, the GPR maps at 600 and 1600MHz frequencies did not reveal, from a visual inspection, a clear spatial correlation with the SWC map, therefore they might affected by other properties, such as porosity or gravel presence.

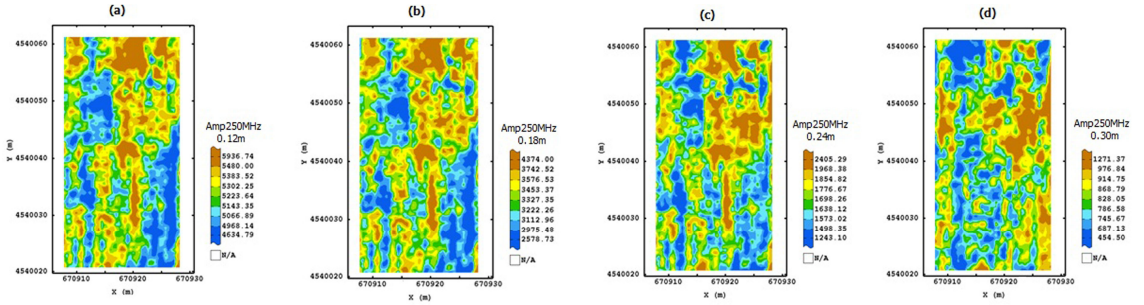

Fig. 4. Maps of estimated amplitude for 250 MHz antenna frequency in July monitoring

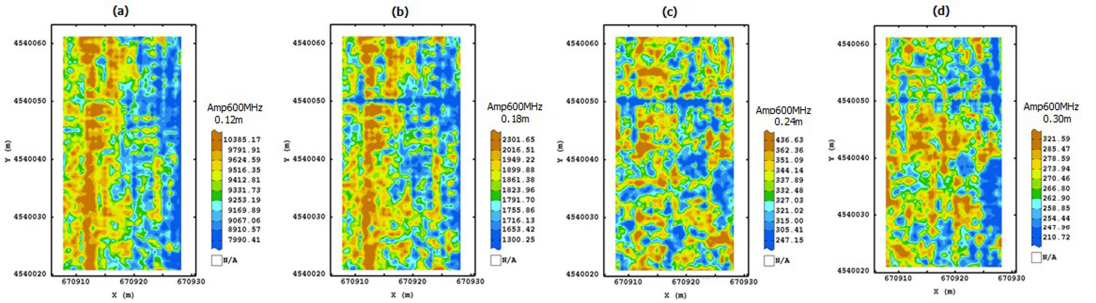

Fig. 5. Maps of estimated amplitude for 600 MHz antenna frequency in July monitoring

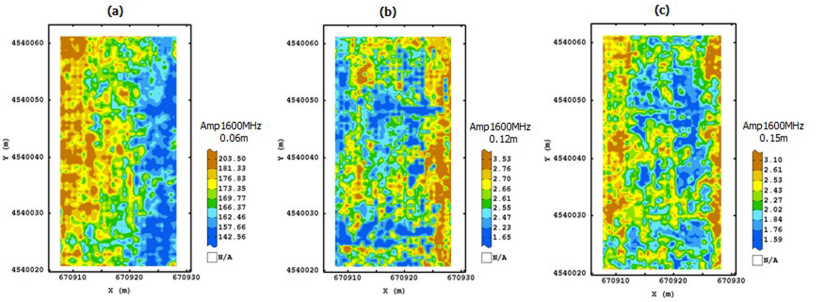

Fig. 6. Maps of estimated amplitude for 1600 MHz antenna frequency in July monitoring.

3.2. Maps of October monitoring

The OK SCW map (Fig. 2b) looked quite similar to the map in July but with higher values.

The EC_{aH} map (Fig. 7a) showed a large area of the plot characterized by higher values. The same spatial structures roughly appeared in the EC_{aV} map (Fig. 7b), through with lower values in the northern area, denoting some discontinuity within about 1-m depth. The area of the plot with higher values of EC_a

corresponded approximately to the zones characterized by higher SWC and silt content, as already observed in July monitoring, which means persistency of the main spatial structures.

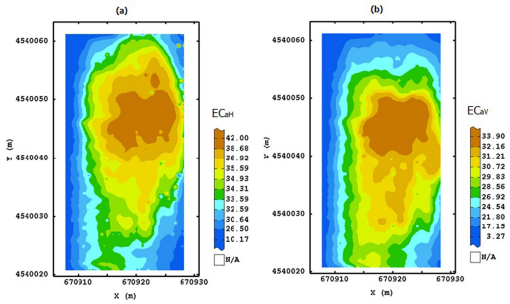

Fig. 7. Spatial estimate of EC_a in October monitoring in horizontal (a) and vertical (b) polarization (in milli-Simiens per meter).

The maps of the estimated amplitude for 250MHz and 600 MHz antenna (Figs. 8 and 9) looked quite similar, except the one at 0.12m for 250MHz antenna, differently from what observed in July monitoring, probably due to an increase of soil uniformity produced by water. The less attenuation of the signal in the northern area might be associated to lower contents of clay.

The maps of the estimated amplitude for 1600MHz antenna (Fig. 10) roughly, delineated three main blocks with a central area characterized by lower values. These results confirm the occurrence in subsoil of scale-dependent variability.

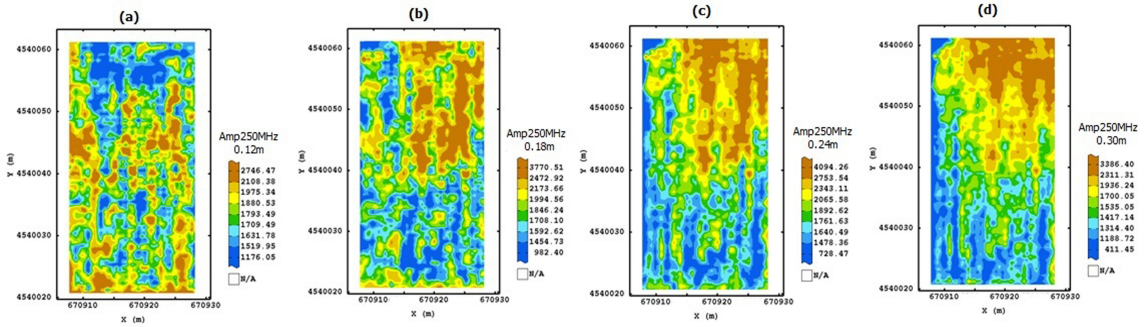

Fig. 8. Maps of estimated amplitude for 250 MHz antenna frequency in October monitoring.

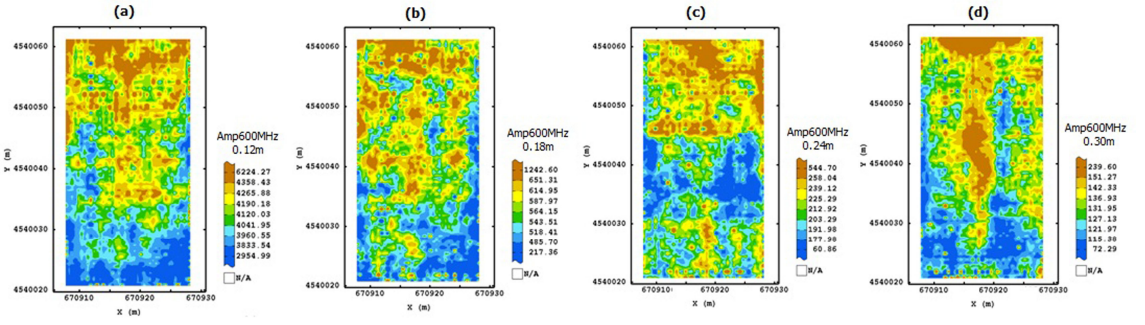

Fig. 9. Maps of estimated amplitude for 600 MHz antenna frequency in October monitoring

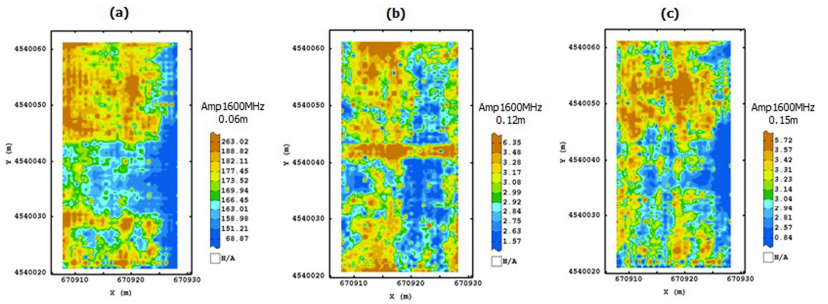

Fig. 10. Maps of estimated amplitude for 1600 MHz antenna frequency in October monitoring.

3.3. Prediction of soil water content

The stepwise regression selected EC_{aH}, 600MHz antenna slices at 0.24 m and 0.30 m depths and 1600 antenna slices at 0.09 m and 0.165 m depths as significant regressors on the SWC in July monitoring with R^2=0.51. Differently in October, the EC_{aH}, 250MHz antenna slices at 0.18 m and 0.30 m depths, 600MHz antenna slices at 0.09 m, 1600MHz antenna slices at 0.075m, 0.12m and 0.135m depths and clay were selected with R^2=0.6. These results highlight that EMI sensor was a useful indicator of shallow SWC at both dates of monitoring, and only some GPR slices of the three antennas.

To estimate the best prediction model for SWC at each date, several alternative models of drift were compared, including the auxiliary variables previously identified by stepwise regression and linear trend in both spatial coordinates (X and Y). At any date the model, realising the smallest mean error rank and the mean squared error, was the one including only the geophysical variables. Once the drift was determined, the estimated generalised covariance was composed only by a nugget effect at any date. The stochastic variation, described by the generalized covariance function, was then not spatially structured and the external drift filtered out all the structured component of spatial variation of SWC.

The results of cross-validation test for both monitoring events (Table 1) showed that the overall performances of OK and KED were quite similar, though KED realized a better correlation with the sample data.

Comparing the maps of SWC at the two dates obtained with KED (Fig. 11) with the ones obtained with OK (Fig. 2), the two types of maps seem to reproduce the same main structures of spatial dependence, even if the KED maps looked more variable. All the maps revealed a wide northern area of higher values, though the KED map in October looked more locally changeable in the southern area.

The increased variability, observed in the KED maps, can be explained since the sub-metre scale information in the geophysical images (Figs. 3-10) was used to downscale the SWC variation. However, it still has to be proved that such variability corresponded to actual variation in SWC.

Table 1. Cross validation test of the estimation of SWC using OK and KED at the two date of monitoring

Date	Estimation method	CV_1	CV_2	CV_3	r
July SWC	OK	0.033	0.99	2.34	0.590
	KED	0.142	1.002	2.37	0.593
October SWC	OK	0.012	0.986	0.92	0.606
	KED	0.028	0.911	0.82	0.709

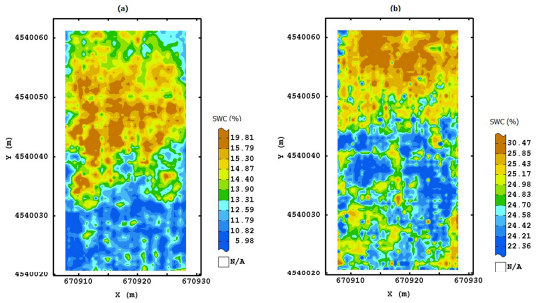

Fig. 11. Spatial estimate of SWC obtained with KED for July (a) and for October monitoring (b).

4. Conclusion

In this study, we focussed on the use of kriging with external drift as a tool to account for geophysical information (EMI and GPR data) as auxiliary information in the prediction of the topsoil water content. The method allowed us to map the soil water content with very few samples at a much higher spatial resolution, using the fine geophysical information, without the need for extensive and expensive direct sampling.

The results did not highlight clear differences among the KED and OK methods: the KED estimates turned out to be more variable and slightly more correlated with the measured values, which tests that SWC was significantly affected by geophysical variation. Kriging with external drift proved to be a valid tool in sensor data fusion and could be effectively applied as technique to fuse data from different sources, in precision irrigation.

References

[1] Galagedara LW, Parkin GW, Redman JD. An analysis of the Ground-Penetrating Radar direct ground wave method for soil water content measurement. *Hydrological Processes* 2003;**17**:3615–3628.
[2] Corwin DL, Lesch SM. Application of soil electrical conductivity to precision agriculture: theory, principles, and guidelines. *Agronomy Journal* 2003;**95**:455–471.
[3] Huisman JA, Hubbard SS, Redman JD, Annan AP. Measuring Soil Water Content with Ground Penetrating Radar: A Review. *Vadose Zone Journal* 2003;**2**:476–491.
[4] Knight R. Ground penetrating radar for environmental applications. *Annu. Rev. Earth. Planet. Sci*. 1997;**29**:299-255.
[5] Bourennane H, King D. Using multiple external drifts to estimate a soil variable. *Geoderma* 2003;**114**:1–18.
[6] Cafarelli B, Castrignanò A. The use of geoadditive models to estimate the spatial distribution of grain weight in an agronomic field: a comparison with kriging with external drift. *Environmetrics* 2011;**22**:769–780.
[7] De Benedetto D, Castrignanò A, Sollitto D, Modugno F, Buttafuoco G, Lo Papa G. Integrating geophysical and geostatistical techniques to map the spatial variation of clay. *Geoderma* 2012;**171-172**:53-63.
[8] Wackernagel H. *Multivariate Geostatistics: an introduction with Applications*. Springer-Verlag, Berlin; 2003.
[9] Soil Survey Staff. Keys to Soil Taxonomy, 11th ed. USDA-Natural Resources Conservation Service, Washington, DC; 2010.
[10] McNeill JD. Electromagnetic Terrain Conductivity Measurement at Low Induction Numbers. Geonics Limited, Technical Note TN 6, Geonics Ltd. Mississauga, Ontario, Canada; 1980.
[11] REFLEX Software. Sandmeier Scientific Software, Karlsruhe, Germany; 2012.
[12] Géovariances. Isatis Technical Ref., ver. 2012.4. Geovariances & Ecole Des Mines De Paris. Avon Cedex, France; 2009.
[13] SAS Institute Inc., Cary, NC, release 9.3; 2012.
[14] Matheron G. The intrinsic random functions and their applications. Advances in Applied Probability 197;**5**:239–465.
[15] Chilès JP, Delfiner P. Geostatistics: Modelling Spatial Uncertainty. Wiley, New York, p. 695; 1999.
[16] Carroll SS, Cressie N. A comparison of geostatistical methodologies used to estimate snow water equivalent. *Water Resource Bulletin* 1996;**32(2)**:267–278.